

Melvinky 1/13

N 70 42102
CR 114228

70-44677

TM-70-2015-5

TECHNICAL MEMORANDUM

LUNAR SURFACE TEMPERATURES
FROM APOLLO 11 DATA

CASE FILE
COPY

Bellcomm

BELLCOMM, INC.

955 L'ENFANT PLAZA NORTH, S.W., WASHINGTON, D.C. 20024

COVER SHEET FOR TECHNICAL MEMORANDUM

TITLE- Lunar Surface Temperatures From
Apollo 11 Data

TM- 70-2015-5

FILING CASE NO(S)- Case 340

DATE- October 5, 1970

AUTHOR(S)- P. J. Hickson

FILING SUBJECT(S)
(ASSIGNED BY AUTHOR(S))-

ABSTRACT

A precision nickel resistance thermometer located outboard on the Early Apollo Science Experiments Package returned good temperature data from the Apollo 11 lunar landing site (Tranquility Base) for one and a half lunar days before the Package ceased operation. The thermometer surface was vertical, faced north, and was 20cm above the lunar surface of which it viewed an area of about 1 square meter. The result of a detailed 270-node thermal analysis of these data is a curve of lunar surface brightness temperature for sun elevation angles between 20 and 165 degrees with a standard error of +4 kelvins at lunar noon. The results are adequately represented by $[(1-\rho) S(\sin\phi)/\sigma]^{1/4}$ where the surface reflectance $\rho = 0.076$, as reported by return-sample analysis, and S is the solar constant, σ is the Stefan-Boltzmann constant and ϕ is the sun elevation. The results are also consistent with the homogeneous moon model of Jaeger with a thermal parameter γ above $500\text{cm}^2\text{-sec}^{1/2}\text{-kelvin/g-cal}$. The available data of the second lunar day reproduce those of the first day within the digitizing error of 1.6 kelvins - so that less than 3%/month dust accretion on the thermometer surface is consistent with these results. The pre-flight thermal data (α, ϵ) were used in the analysis, the results of which were not affected by adding up to 7% (theoretical) dust to the thermometer surface. This is consistent with negligible accumulation of dust on the thermometer during Lunar Module ascent.

BA-145A (8-68)

SEE REVERSE SIDE FOR DISTRIBUTION LIST

DISTRIBUTIONCOMPLETE MEMORANDUM TO

CORRESPONDENCE FILES:

OFFICIAL FILE COPY

plus one white copy for each
additional case referenced

TECHNICAL LIBRARY (4)

NASA Headquarters

R. J. Allenby/MAL
D. A. Beattie/MAL
R. G. Brereton/MAL
L. J. Casey/MAT
E. Heer - MAL
J. B. Hanley/MAL
L. J. Kosofsky/MAL
A. S. Lyman/MR
B. Milwitsky/MA
W. T. O'Bryant/MAL
L. R. Scherer/MAL
A. J. Schwarzkopf/MAP-1
W. E. Stoney/MA

Langley Research Center

T. W. E. Hankinson/159
W. S. Slemp/187

Manned Spacecraft Center

J. R. Bates/TG5
A. J. Calio/TA
A. B. Carraway/TD2
S. C. Freden/TG
P. D. Gerke/TD3
D. H. Greenshields/ES5
H. R. Greider/TD3
R. S. Harris/ES16
B. G. Jackson/TD
R. S. Johnston/AC
G. P. Kenney/TD5
W. K. Stevenson/TD4
D. G. Wiseman/TD

COMPLETE MEMORANDUM TOMarshall Space Flight Center

B. P. Jones/4481
J. K. Harrison/PD-MP-P

Bell Telephone Laboratories

D. B. James

Bendix Aerospace - Ann Arbor

J. Dye
P. Georgopoulos
J. McNaughton
K. More
G. Psaros
R. Sims
C. Weatherred

Boeing Scientific Research
Laboratories

J. M. Saari
R. W. Shorthill

Hughes Aircraft Corporation

R. R. Garipay

Jet Propulsion Laboratory

J. E. Conel/183-501
W. A. Hagemeyer/157-507
J. W. Lucas/157-205
J. W. Smith/157-507
L. D. Stimpson/157-507
Z. Popinski/157-410

Lamont-Doherty Geological
Observatory

M. Langseth
G. Latham

Massachusetts Inst. of Tech.

G. Simmons

Northrop Corporation

G. Vitkus

Spectrolab Inc.

J. D. Gum
E. D. Steele

BELLCOMM. INC.

DISTRIBUTION LIST (CONT'D)

COMPLETE MEMORANDUM TO (CONT'D)

Tylan Corporation

D. B. LeMay

University of Maryland

C. O. Alley

D. J. Currie

University of Sydney

B. J. O'Brien

Bellcomm, Inc.

G. M. Anderson

D. R. Anselmo

D. O. Baechler

I. Y. Bar-Itzhack

A. P. Boysen, Jr.

J. O. Cappellari, Jr.

K. R. Carpenter

D. A. Corey

S. S. Fineblum

J. H. Fox

D. R. Hagner

W. G. Heffron

J. J. Hibbert

N. W. Hinners

T. B. Hoekstra

A. N. Kontaratos

M. Liwshitz

H. S. London

P. F. Long

D. Macchia

E. D. Marion

J. L. Marshall

R. E. McGaughy

J. Z. Menard

J. M. Nervik

J. J. O'Connor

M. P. Odle

G. T. Orrok

J. W. Powers

P. E. Reynolds

COMPLETE MEMORANDUM TO (CONT'D)

Bellcomm, Inc. (Cont'd)

J. A. Saxton

J. A. Schelke

P. F. Sennewald

E. N. Shipley

R. V. Sperry

W. B. Thompson

J. W. Timko

A. R. Vernon

J. E. Volonte

R. L. Wagner

J. E. Waldo

D. B. Wood

G. M. Yanizeski

All Members Department 2015

Department 1024 File

Abstract Only to

Bellcomm, Inc.

J. P. Downs

I. M. Ross

M. P. Wilson

BELLCOMM, INC.

955 L'ENFANT PLAZA NORTH, S.W. WASHINGTON, D. C. 20024

SUBJECT: Lunar Surface Temperatures From Apollo 11 Data - Case 340

DATE: October 5, 1970

FROM: P. J. Hickson

TM-70-2015-5

TECHNICAL MEMORANDUM

I. Introduction

The Early Apollo Science Experiments Package (EASEP) was emplaced on the lunar surface by an Apollo 11 astronaut during the first lunar landing in Mare Tranquillitatis. EASEP was a solar-powered, condensed version of the standard nuclear-powered Apollo Lunar Surface Experiments Package (ALSEP), to be deployed as a multi-experiment observatory at each lunar landing site. In addition to a scientific experiment, a seismometer, EASEP contains an engineering experiment (Dust, Thermal, and Radiation Engineering Measurement, DTREM I) consisting of a set of six sensors to measure the lunar environment.

One of the sensors, a precision nickel resistance thermometer of wide dynamic range, is mounted vertically and is facing outboard of EASEP so that a good view of the lunar surface is obtained. Analysis of the nickel thermometer data obtained during the lunar daytime yields an average brightness temperature of the lunar surface area viewed. Apollo 14 and 15 ALSEP's will carry an improved version, designated DTREM II, which will yield lunar nighttime temperatures as well. DTREM II will have an unobstructed view of the lunar surface and carry an extra thermometer to measure the heat leaks from the brightness thermometer.

In his recent review article on the infrared moon R. W. Shorthill (Reference 1) comments that data on the nighttime temperature of the moon is incomplete, since such data is difficult to obtain from earth. The Surveyor spacecraft were equipped with batteries as well as solar panels, but only limited in-situ thermal data were obtained after sunset. The Apollo DTREM measurements were conceived as a spatial extension of the Surveyor results to other landing sites, from which ground-truth in the form of return rock samples would be available, and as a temporal extension to nighttime phase angles over many complete lunations. The Apollo program permitted some attention to thermometer errors; therefore, the experiment design provides insulation not available to the Surveyor experimenters, and an increase in brightness temperature accuracy is expected.

II. Sketch of the Experiment

Figures 1 and 2 are sketches of the DTREM I package indicating the thermal isolation and thermal finish of

the thermometer. Figure 3 shows the DTREM I location on EASEP, and Figure 6 is a plot of all the official data.

The lunar surface brightness temperature is found from the nickel thermometer energy-rate balance, i.e., the net rate of energy flow out of the detector is equal to the net rate of energy flow into the detector. We write this equation in the form:

$$\epsilon_{Ni} \sigma T_{Ni}^4 = \epsilon_{Ni} F_{NiS} \epsilon_S \sigma T_S^4 + \dot{q}/A_{Ni} \quad (1)$$

where ϵ is the emissivity, σ is the Stefan-Boltzmann constant, T is the absolute temperature, F the geometric view factor, Ni stands for nickel resistance thermometer, S stands for lunar surface, and \dot{q}/A_{Ni} is the net algebraic sum, divided by the thermometer area, of all heat leaks and heat inputs to the thermometer and of the rate of internal energy storage in the thermometer. The latter is, however, negligible and a steady state analysis was carried out. The geometric view factor F_{NiS} is defined, by reciprocity, as $(A_S/A_{Ni}) F_{SNi}$ where F_{SNi} is the fraction of the radiant energy emanating from finite surface area A_S which is intercepted by another finite surface A_{Ni} . The heat leaks and heat inputs to the thermometer include reflections and emissions from all nearby surfaces of the EASEP spacecraft, and conduction from the DTREM housing to the nickel thermometer. The geometric view factors of the thermometer to the various surfaces are listed in Table I. Since T_{Ni} is measured and the terms of \dot{q}/A_{Ni} are measured or can be calculated from other EASEP spacecraft housekeeping temperatures, the lunar surface brightness temperature, defined as T_S for $\epsilon_S = 1$, is found at each sun angle from Equation(1) with F_{NiS} and \dot{q} adjusted to the sun angle.

The EASEP geometry is fairly complex, but careful thermal analysis and detailed calculation of the appropriate corrections yield, in principle:

1. an average equivalent brightness temperature of the unshadowed lunar surface viewed,
2. an equivalent range of the surface thermal parameter $(k\rho c)^{-1/2}$, where k is the thermal conductivity, ρ is the mass density and c is the heat capacity of the lunar surface layer, and
3. the angular dependence of the lunar surface thermal emission.

Results of this type were reported previously by J. W. Lucas et al (Reference 2) for all landed Surveyor spacecraft.

Moreover, comparison of data from successive months may yield the degradation rates of the thermal coatings used or viewed. Note however that the EASEP thermometer is mounted vertically, facing north, so that direct sun viewing is avoided and coating degradation is expected to be small. Also, the third objective above was not met, i.e., the angular dependence of the lunar surface thermal emission could not be determined from the EASEP because the thermometer faces north, normal to the sun-to-surface direction, the very direction which in previous measurements has been shown to be the important one (Reference 3). The future ALSEP data should yield more complete results.

III. Description of the Instrument

The thermometer used in the experiment is a nickel wire resistor made by the Tylan Corporation. The resistor, which has a nominal 5500 ohm resistance at the ice point, is connected to ground and also through a 15000 ohm temperature-insensitive precision dropping resistor to the +12 volt $\pm 1\%$ regulated EASEP power line, as seen in Figure 8. The thermometer voltage drop is fed to the EASEP 8-bit analogue-to-digital converter and is measured once every 54 seconds. The voltage of the +12 volt supply is measured 4 seconds before each temperature is measured and so introduces only a small ($<1/4\%$) measurement error. The thermometer has a dynamic range of 84K (-308°F) to 408K (274°F) and the ΔT corresponding to 1/2 bit is almost constant at 0.8 kelvins over this entire range. According to the manufacturer, the calibration of the thermometer to an absolute temperature scale is accurate to at least 0.8 kelvins over the entire range since three calibration points, the steam point, the ice point and the carbon dioxide point are taken for each sensor. The thermometer and its circuit have good stability characteristics and drift less than 0.1 kelvins/year.

For proper understanding of the thermal analysis a detailed description of the instrument configuration is necessary. Figure 7 is an exploded view of the thermometer showing its laminated construction and internal radiation shields; when bonded together the sandwich is 0.9mm thick. The DTREM package, shown pictorially in Figure 1 and in exploded view in Figure 2, is a cube of G-10 fiberglass, 36x32x41mm, with walls 2.3mm thick. The top of the package is covered by a kovar sheet to which three 10x20mm solar cells are attached for the dust and radiation measurements, conducted by Dr. S. Freden of the Manned Spacecraft Center and Dr. B. O'Brien of the University of Sydney (Reference 4). This kovar sheet has two thermistors attached underneath, which are on scale only above 305 K. The solar cell outputs are used in the thermal analysis to give the

insolation directly, since parts of the EASEP spacecraft shadow the DTREM package as seen in Figure 6. The north face of the DTREM package is covered by the nickel thermometer but separated from it by 20 layers of superinsulation (about 2mm thick), which are pierced by a pair of thermal isolator standoffs and nylon bolts. The DTREM is held by 2 bolts to an insulating fixture attached to the EASEP primary structure.

Figures 3, 4, and 5 show the deployed configuration of EASEP, almost due south of the landed Lunar Module and 18 meters from it (Reference 5). The deployed EASEP is level ($\pm 1/2^\circ$), facing a slight, 4 degree, slope inclined upward toward the Lunar Module. The laser experiment array is 4 meters distant to the northwest.

IV. Description of the Data Analysis

As indicated in Section II, above, the nickel thermometer temperatures are reduced to lunar surface brightness temperatures once the power inputs to the thermometer from all sources other than the lunar surface are calculated and added algebraically. The calculation of these inputs requires a knowledge of the lunar surface temperature, and so an iterative technique must be used. Also, the insulating qualities of the DTREM package and of the thermometer laminates require a multinode analysis to deal with the large thermal gradients. The high lunar vacuum ensures that the heat transfer is dominated by the thermal radiation.

The method used is as follows: The geometric view factors from the thermometer to various parts of EASEP were calculated by the standard computer program CONFAC (Reference 6) and are listed in Table I; these required only knowledge of the EASEP geometry. From the EASEP geometry and orientation the dimensions of its shadow on the lunar surface were obtained, hence the geometric view factor from the thermometer to the sunlit lunar surface, F_{NiS} , for each sun elevation, as given in Figure 9 was calculated. The DTREM package was then divided into 270 thermal nodes for steady state analysis and the thermal analysis computer preprocessor Chrysler Improved Numerical Differential Analyzer (CINDA, Reference 7) and its subroutines were used to write a FORTRAN computer program that solves the thermal network, that is, calculates the equilibrium temperature of every node. For each sun elevation the FORTRAN program is given 8 EASEP temperatures, including the nickel thermometer temperature, and the geometric view factors. A lunar surface temperature is assumed, and each side of Equation (1) is calculated using the iterative subroutine CINDSM. If the calculated values on either side of Equation (1) do not agree within acceptable limits, a new lunar surface temperature is assumed and the CINDSM analysis is repeated. This iteration is continued until an acceptable energy rate balance is obtained for the nickel thermometer with its temperature fixed at the measured value. As indicated, the above iteration is repeated for selected values of sun elevation angle.

The EASEP temperatures used as input to the analysis were from thermometers on the east, west, and bottom of the EASEP primary structure (the 1.2mm thick aluminum box in contact with the lunar surface), on the east and west solar panels, on the northeast and northwest of the central station thermal plate, on the DTREM kovar sheet (when on scale), and the DTREM nickel thermometer (see Figures 2 and 3). The temperature of the dark lunar surface was taken as 200 K. Since a value of 0.076 for the lunar surface reflectance ρ was measured on an Apollo 11 soil sample (Reference 8), the initial value of the (iterated) lunar surface temperature was taken to be $[(1-\rho) S(\sin\phi)/\sigma]^{1/4}$ where S is the solar constant and ϕ the sun elevation.

The heat rate balance for the nickel thermometer coil of wire then included: radiation from the black sky, the sunlit lunar surface, the dark lunar surface, the west side of the bracket, the back of the bracket, the boom, astronaut handle and carry handle, the east solar panel, the west solar panel, and both parts of the rock;* a conduction contribution from 8 nodes on the laminated part of the thermometer and Joule heating; and direct solar input to the thermometer due to the specific sun-DTREM geometry and sunlight reflection from the lunar surface, the bracket, and the back of the solar panels. The calculation of inter-node conductances and the heat rate input to each node was not unusual; the constants used in the analysis are given in Table II. Of interest may be the fact, mentioned above, that calibrated solar cell outputs were available as measured insolation on the DTREM package so that calculation of EASEP shadow dimensions on the DTREM structure was unnecessary. The algebraic sum of these heat rates should be zero and iteration was continued until the sum was less than 1/2% of the lunar surface input. These heat rates, grouped into nine independent partial sums, divided by the heat rate from the sunlit lunar surface, are plotted in Figure 10.

Referring to Figure 10 we see that, aside from the black sky, the largest correction to the data is from the EASEP bracket, typically 30% but rising to 120% at low sun elevation. In estimating the lunar surface temperature error we assume that the calculated corrections of Figure 10 are independent and are accurate to a 10% relative 1 sigma error. Then, since the relative temperature error is 1/4 of the relative error in the radiated energy, we estimate the temperature error (1 sigma) to be +4 kelvins at 90° sun elevation and +20 kelvins at 20° sun elevation.

The calculated lunar surface brightness temperature is given in Figure 11 with the estimated error indicated. A curve of $[(1-\rho)S(\sin\phi)/\sigma]^{1/4}$, the Lambert temperature** for

*This is the split rock so evident in Figures 4 and 5.

**The Lambert temperature is the temperature a perfectly insulating Lambert surface with unit emissivity would come to if it absorbed the same amount of radiation as the surface under consideration." (Reference 1).

$\rho = 0.076$, is also given in Figure 11 for comparison.

As an illustration of the calculated temperatures we note that at a sun elevation of 20° the sun is at 70° incidence to the east face of the DTREM package, while the solar cell thermistors on top are not yet on scale and the west face is, of course, completely in shadow. At this sun elevation the nickel temperature is 273 K, while other nodes on the thermometer range from 10 kelvins above this to 0.3 kelvins below. The north face of the DTREM package is typically 5 kelvins hotter, the east face 19 kelvins hotter (the range is 10 to 60 kelvins) the top solar cells 45 kelvins hotter and the west face about 20 kelvins colder. These numbers illustrate the advantage of an additional thermometer to measure the conductive leak from the nickel thermometer.

V. Results of the Measurement

The nickel thermometer data from Apollo 11 is given in Figure 6 and the lunar surface brightness temperatures calculated from these data are given in Figure 11 with the estimated 1 sigma errors. The Lambert temperatures for a reflectance of 0.076, given in Figure 11, are seen to adequately represent the brightness temperatures. Table III lists Lambert temperatures for selected values of the sun elevation as well as theoretical values of lunar surface temperatures calculated with the homogenous-moon model of Jaeger (Reference 9), for various values of thermal parameter $\gamma = (k\rho c)^{-1/2}$. Comparison of Figure 11 and Table III suggests that the results are adequately represented by the homogeneous model for any value of γ greater than $500\text{cm}^2\text{-sec}^{1/2}\text{-kelvin/g-cal}$. The Surveyor results are usually higher than 500, ranging up to about 1000. Table III includes also a number of predicted temperatures for angles after sundown (assuming no temperature dependence of thermal conductivity k or volumetric heat capacity ρc), to point out the relative insensitivity of the daytime data to γ and the distinct advantage of lunar night data for discriminating between γ values.

Figure 9 shows depressions in the thermometer-to-sunlit surface geometric view factor at low sun angles. These depressions are the result of shadows of the solar panels on the lunar surface. Note that, of the total value of 0.38 for the geometric view factor, fully 74% is attributable to the lunar surface between EASEP and the end of the solar panels, an area of about 1 square meter which is clearly visible in Figure 5, and to a lesser degree in Figure 4. This surface is seen to be reasonably flat and free of boulders and depressions although it has a number of foot-imprints.

As mentioned in Section II, comparison of nickel temperatures from successive lunations was expected to bear on the

degradation of thermal finishes used or viewed, degradation due to ultraviolet damage to the paint and/or dust accretion on the paint. We observe that the available data of the second lunation reproduces that of the first day within the digitizing error of 1.6 kelvins and conclude therefore that negligible dust accretion during the first 30 days of operation is consistent with these observations. To quantify this result we note that 1.6 kelvins corresponds to a 1.6% change in the lunar surface input to DTREM at lunar noon, or equivalently, corresponds to a 10% change in absorptivity or an absolute change of 0.03, possible due to the addition of 3% dust. A dust accretion rate lower than 3%/month is not surprising. Also, degradation of the thermometer surface by ultraviolet light is not expected at the low irradiation exposure of north-facing surfaces.

The pre-flight thermal data (α, ϵ) were used in the analysis, the results of which were not affected by adding up to 7% (theoretical) dust to the thermometer surface, i.e., our results are also consistent with negligible dust accumulation on the thermometer during Lunar Module ascent. To quantify this result we assume that if the inferred lunar temperatures were all high, which implies at least a 1 sigma increase, we should attribute this increase to changes in our pre-flight thermal parameters. The 1 sigma or 4 kelvins increase would correspond to 7% dust cover. These results imply that the nickel thermometer does not have good resolution for dust detection, either for absolute determination or for detection of short term changes.

VI. Acknowledgement

Miss M. P. Odle assisted greatly in the computer programming.



P. J. Hickson

2015-PJH-bab

Attachments
References
Tables
Figures

References

1. Shorthill, Richard W., "The Infrared Moon: a Review", Journal of Spacecraft and Rockets, Volume 7, p. 385, (1970).
2. Stimpson, L. D., Hagemeyer, W. A., Lucas, J. W., Popinski, Z; Saari, J. M., "Lunar Surface Temperatures and Thermal Characteristics Revised from Surveyor Spacecraft Data", Journal of Geophysical Research, to be published.
3. Montgomery, C. G., Saari, J. M., Shorthill, R. W., and Six, N. F., "Directional Characteristics of Lunar Thermal Emission", Technical Note R-213, Research Laboratories, Brown Engineering Company, Inc. Huntsville, (November 1966).
4. Bates, J. R., Freden, S. C., and O'Brien, B. J., "The Modified Dust Detector in the Early Apollo Scientific Experiments Package", p. 199, in NASA SP-214, The Apollo 11 Preliminary Science Report, (1969).
5. Shoemaker, E. M., Bailey, N. G., Batson, R. M., Dahlem, D. H., Ross, T. H., Grolier, M. J., Goddard, E. N., Hait, M. H., Holt, H. E., Larson, K. B., Rennilson, J. J., Schaber, G. G., Schleicher, D. L., Schmitt, H. H., Sutton, R. L., Swann, G. A. Waters, A. C., and West, M. N., "Geologic Setting of the Lunar Samples Returned by the Apollo 11 Mission", p. 41 in NASA SP-214, The Apollo 11 Preliminary Science Report, (1969).
6. Toups, K. A., "A General Computer Program for the Determination of Radiant-Interchange Configuration and Form Factors - CONFAC II", Technical Report SID 65 1043-2, North American Aviation, Inc. Space and Information System Division, (October, 1965).
7. Lewis, D. R., Gaski, J. D., and Thompson, L. R. "Chrysler Improved Numerical Differencing Analyzer for 3rd Generation Computers", Technical Note TN-AP-67-287, Chrysler Corporation Space Division, New Orleans, (October 20, 1967).
8. Birebak, R. C., Cremis, C. J., and Dawson, J. P., "Thermal Radiation Properties and Thermal Conductivity of Lunar Material", Science Vol. 167, p. 724 (1970).
9. Jaeger, J. C., "Conduction of Heat in a Solid With Periodic Boundary Conditions, with an Application to the Surface of Temperature of the Moon", Proc. Camb. Phil. Soc. 49 p. 355, (1953).

TABLE I

Geometric View Factors from the Nickel
Thermometer to Various Surfaces of EASEP*

Surface	Geometric View Factor
lunar surface	0.387**
black sky	(0.312)***
bracket, carry handle	0.160
boom, astronaut handle	0.049
west solar panel	0.025
rock, east part	0.014
rock, west part	0.025
LM descent stage	0.004
laser experiment array	0.012
east solar panel	0.012
	<u>1.000</u>

* See Figure 3

** Includes shadowed and unshadowed lunar surface. The sunlit lunar surface has a geometric view factor, depending on sun angle (see Figure 9), between 0.099 and 0.387. The geometric view factor to the shadowed lunar surface is 0.387 diminished by the view factor to the sunlit surface.

*** An effective value for the black sky view factor of 0.418 was used, in agreement with Equation (1).

TABLE II

Constants used in Thermal Analysis

	absorptivity α	emissivity ϵ	conductivity k mW/m-kelvin
S-13G thermal paint	0.288	0.885	350
solar cell	0.81	0.83	
kovar (painted)	0.90	0.90	
solar panel (back)	0.3	0.3	
rock	1.0	1.0	
dust	1.0	1.0	
G-10 fiberglass, nylon			350
Vespel			380
aluminum			116,800
kovar			29,700
nickel			62,300
<p>solar constant $S = 1350. \text{ W/m}^2$</p> <p>Stefan-Boltzmann constant $\sigma = 5.670 \times 10^{-8} \text{ W/m}^2 - \text{K}^4$</p> <p>reflectance of lunar surface $\rho = 0.076$</p> <p>sun declination, degrees $1.3 - 0.022 (\text{DAY}-200)$</p> <p>Apollo 11 longitude, latitude $23^\circ.48, + 0^\circ.663$</p>			

TABLE III

Theoretical Lunar Surface Brightness Temperatures, in degrees Kelvin, for selected values of the Sun Elevation Angle and the Thermal Parameter $\gamma = (k\rho c)^{-1/2}$ in $\text{cm}^2 \cdot \text{sec}^{1/2} \cdot \text{kelvin/g-cal}$.

Sun Elevation degrees	Lambert Temperature, K $\rho = 0.076$	Thermal Parameter γ			
		250	500	750	1500
10	244 K	228 K	236 K	240 K	244 K
20	289	284	289	291	292
30	318	317	320	321	322
90	378	383	384	384	385
150	318	324	324	324	324
160	289	297	295	295	295
170	244	257	253	252	250
180		183	161	149	130
190		165	143	131	112
270		133	114	104	88
360		122	104	94	80

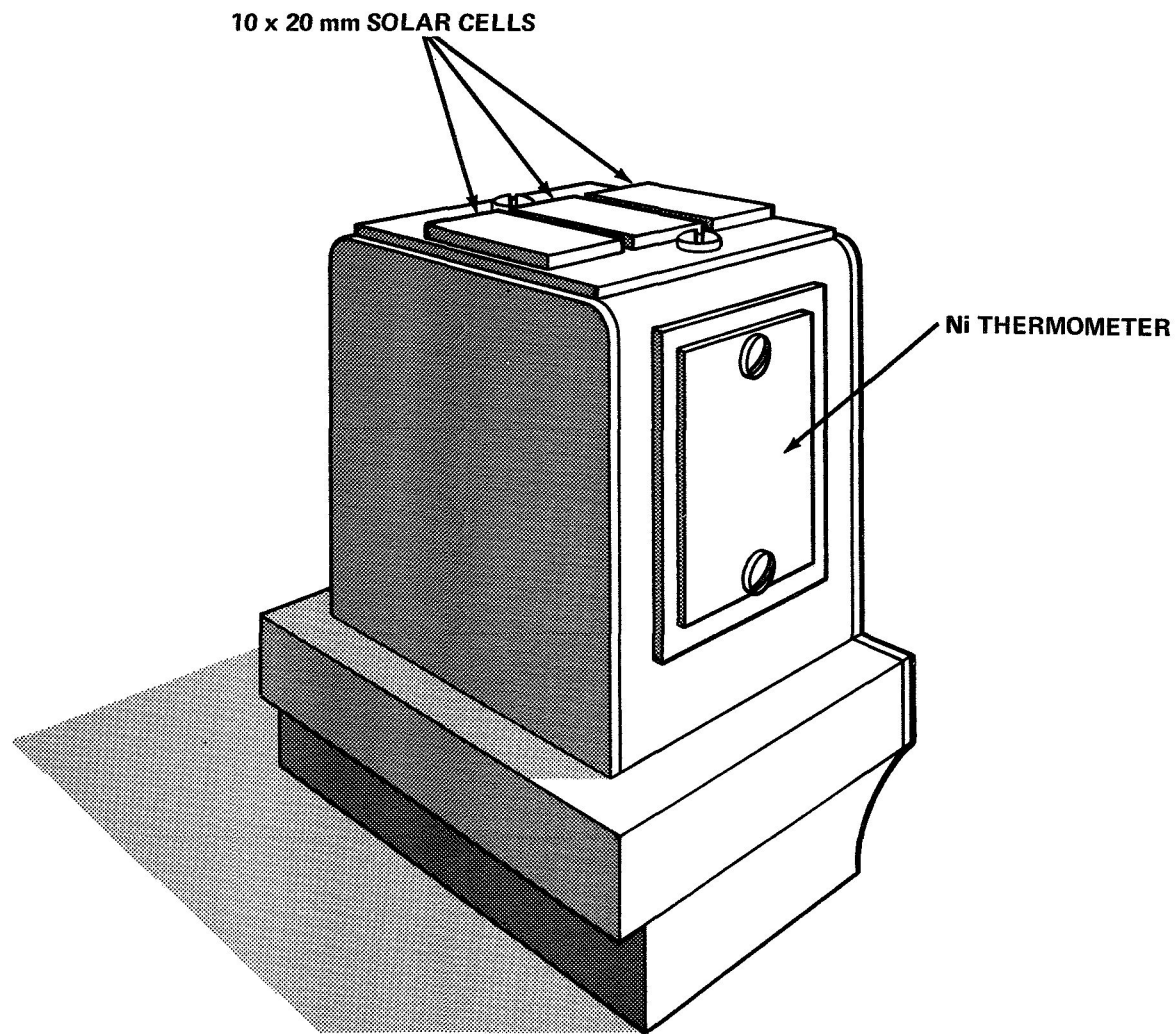


**FIGURE 1- DUST, THERMAL, AND RADIATION ENGINEERING MEASUREMENT PACKAGE (DTREM I)
AS ON EASEP/APOLLO 11 AND ON ALSEP OF APOLLO 14 AND 15.**

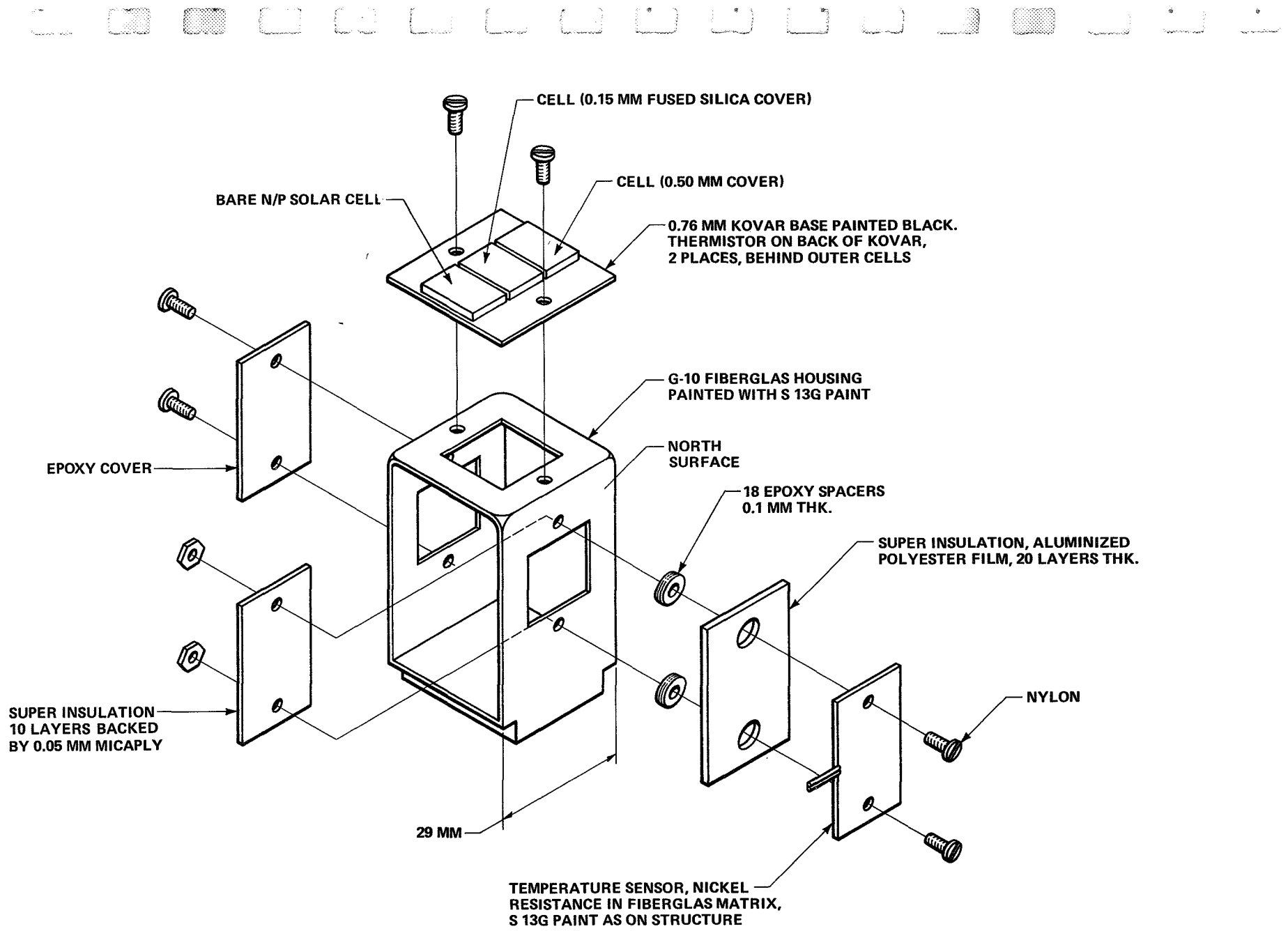


FIGURE 2 - DTREM 1 AS ON EASEP OR APOLLO 11. (DUST, THERMAL AND RADIATION ENGINEERING MEASUREMENT OR MODIFIED DUST DETECTOR EXPERIMENT), THERMAL DETAILS

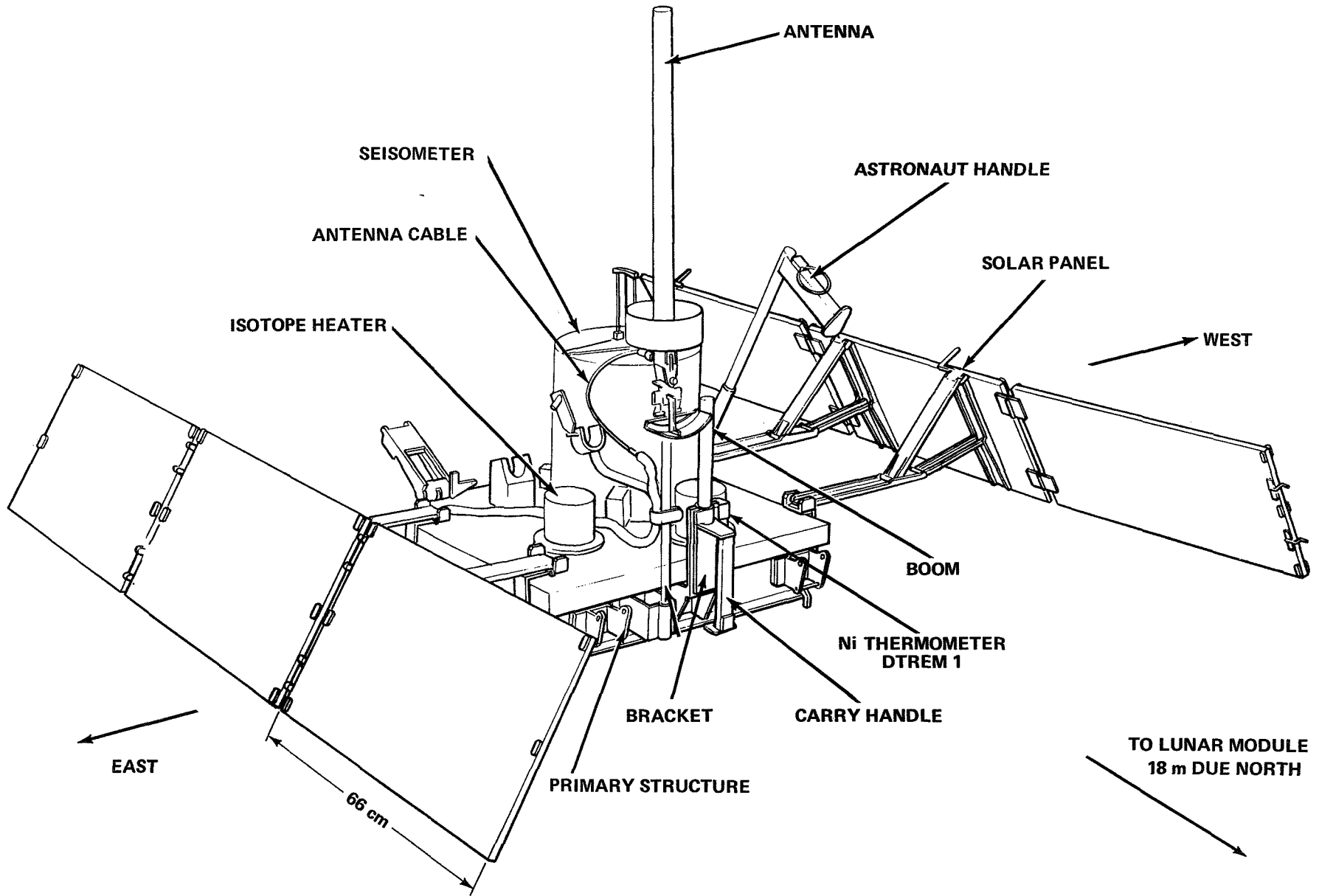


FIGURE 3 - EARLY APOLLO SCIENCE EXPERIMENT PACKAGE (EASEP) SHOWING DTREM 1 GEOMETRY

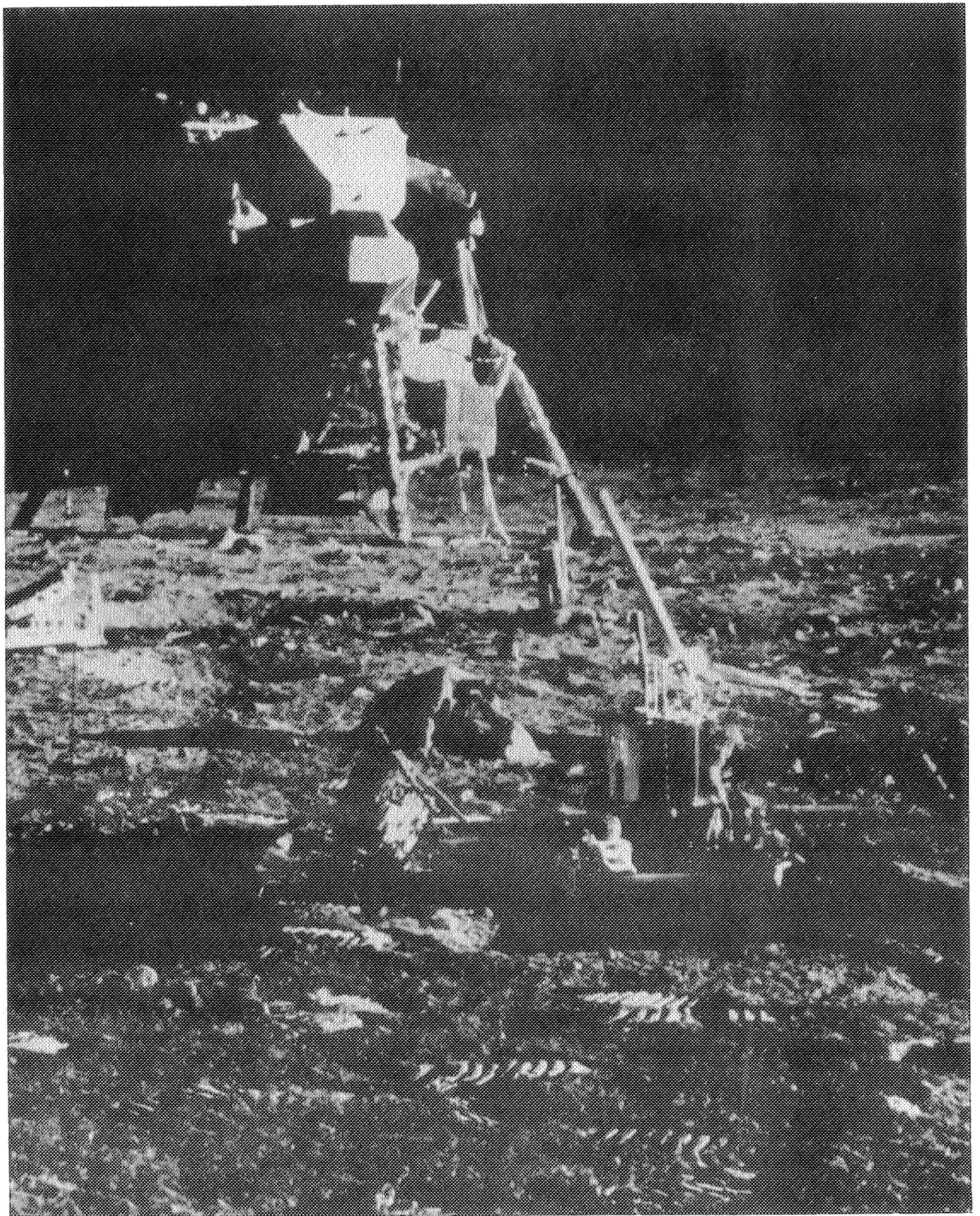


FIGURE 4 - EASEP, DEPLOYED CONFIGURATION, SHOWING THE LUNAR MODULE (18 m DUE NORTH), THE LASER EXPERIMENT ARRAY, AND THE "ROCK": NOTE THE LUNAR SURFACE NORTH OF EASEP BETWEEN THE SOLAR PANELS.

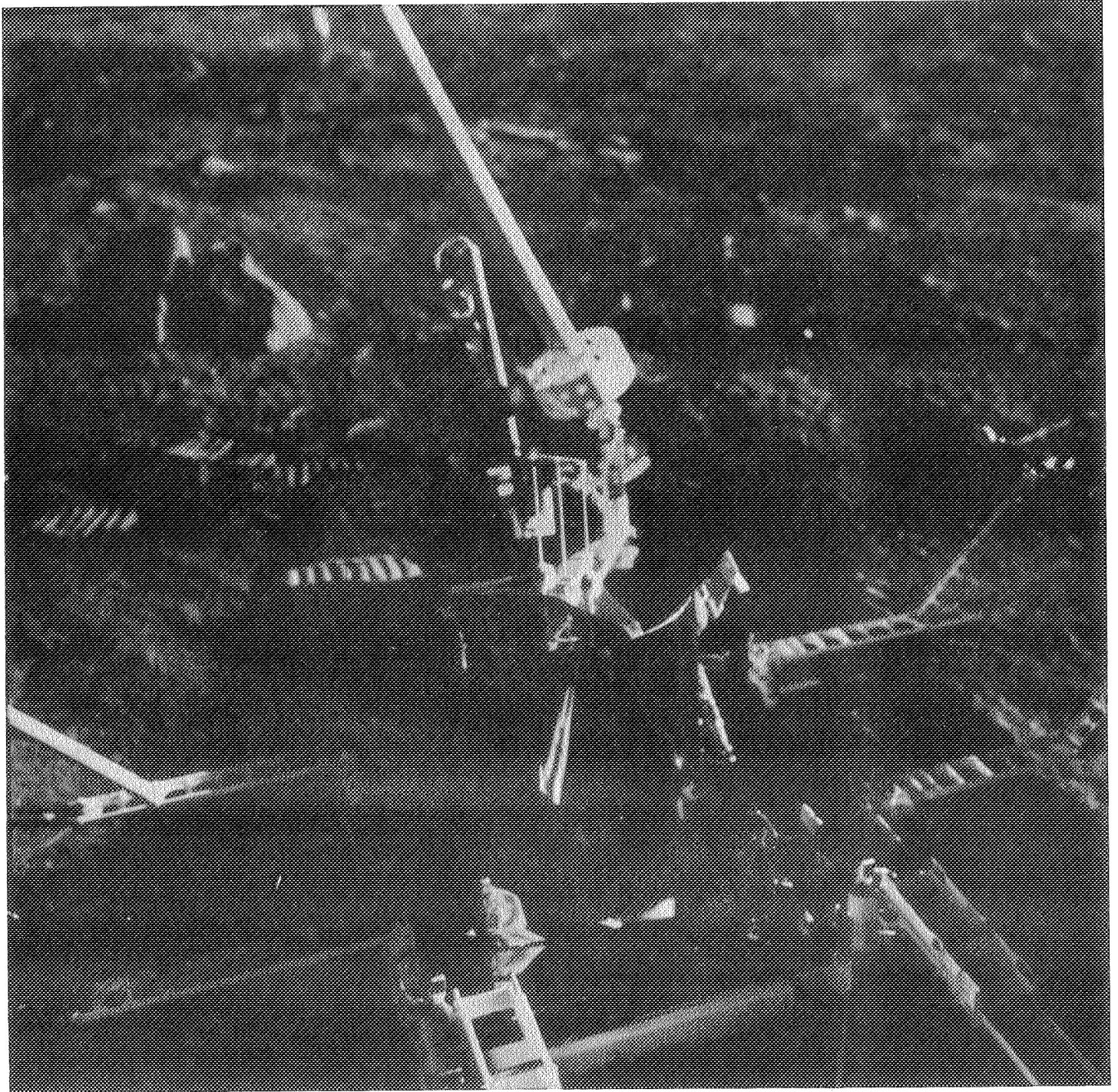


FIGURE 5 - EASEP, DEPLOYED CONFIGURATION, SHOWING SOLAR PANELS, ANTENNA, SEISMOMETER, AND ROCK. THE NICKEL THERMOMETER OF DTREM I VIEWS THE LUNAR SURFACE BETWEEN THE SOLAR PANELS OUT TO THE ROCK

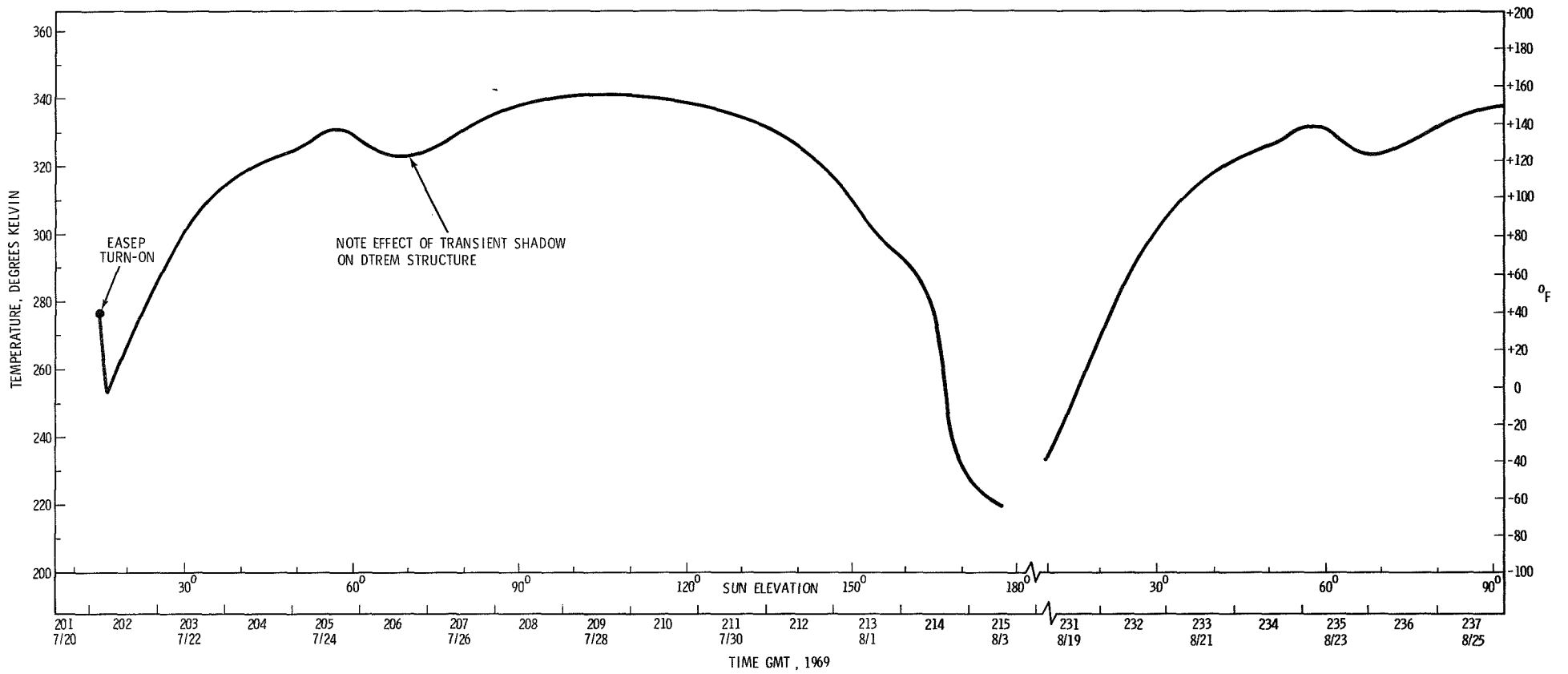
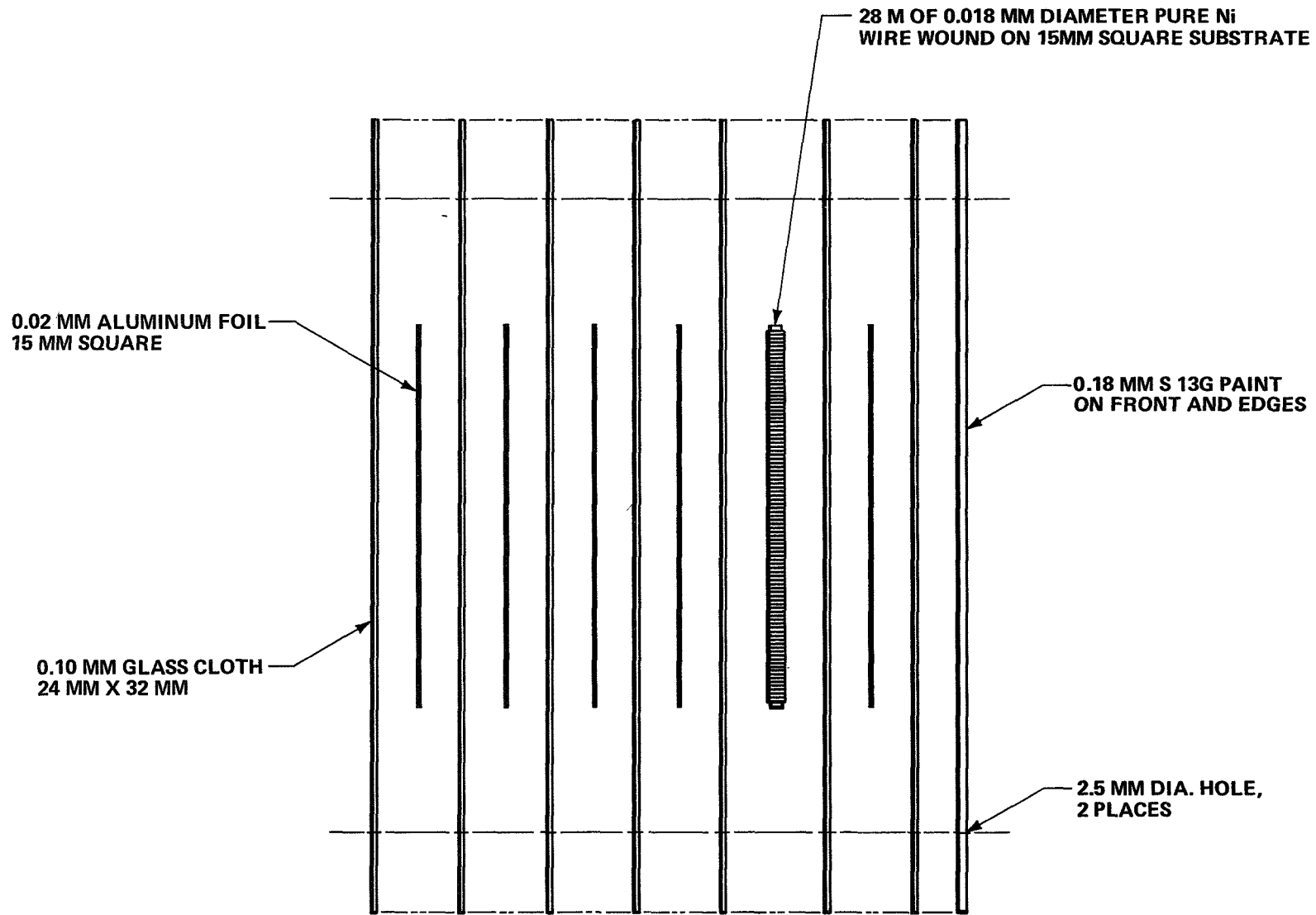


FIGURE 6 - DTREM I Ni THERMOMETER TEMPERATURE FROM EASEP DATA



**FIGURE 7 - FIBERGLASS NICKEL RESISTANCE THERMOMETER,
EXPLODED VIEW. (EPOXY BINDER NOT SHOWN)**

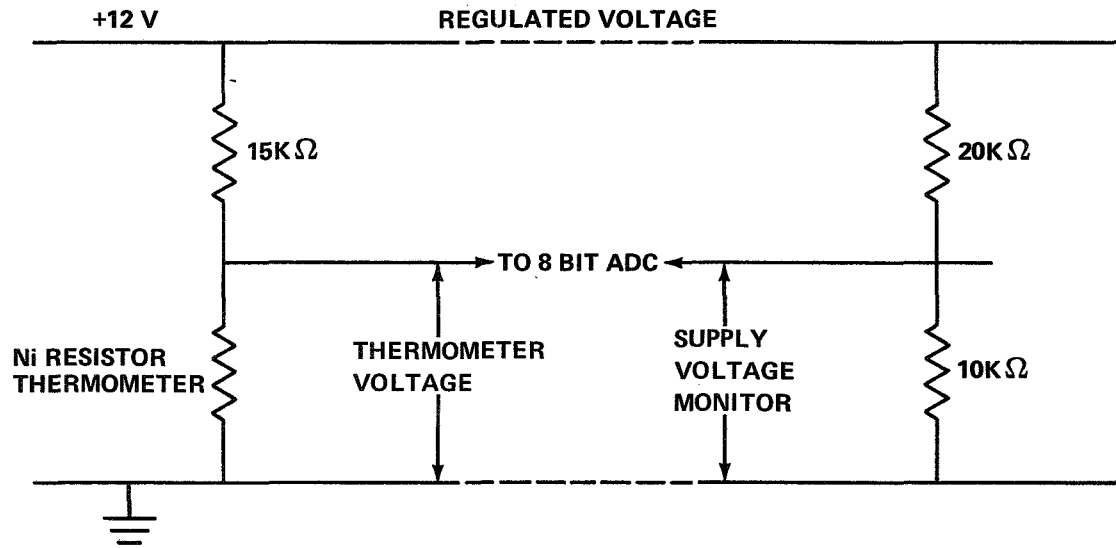


FIGURE 8 - THERMOMETER SCHEMATIC CIRCUIT DIAGRAM (ALL PRECISION RESISTANCES < 25 ppm kelvin)

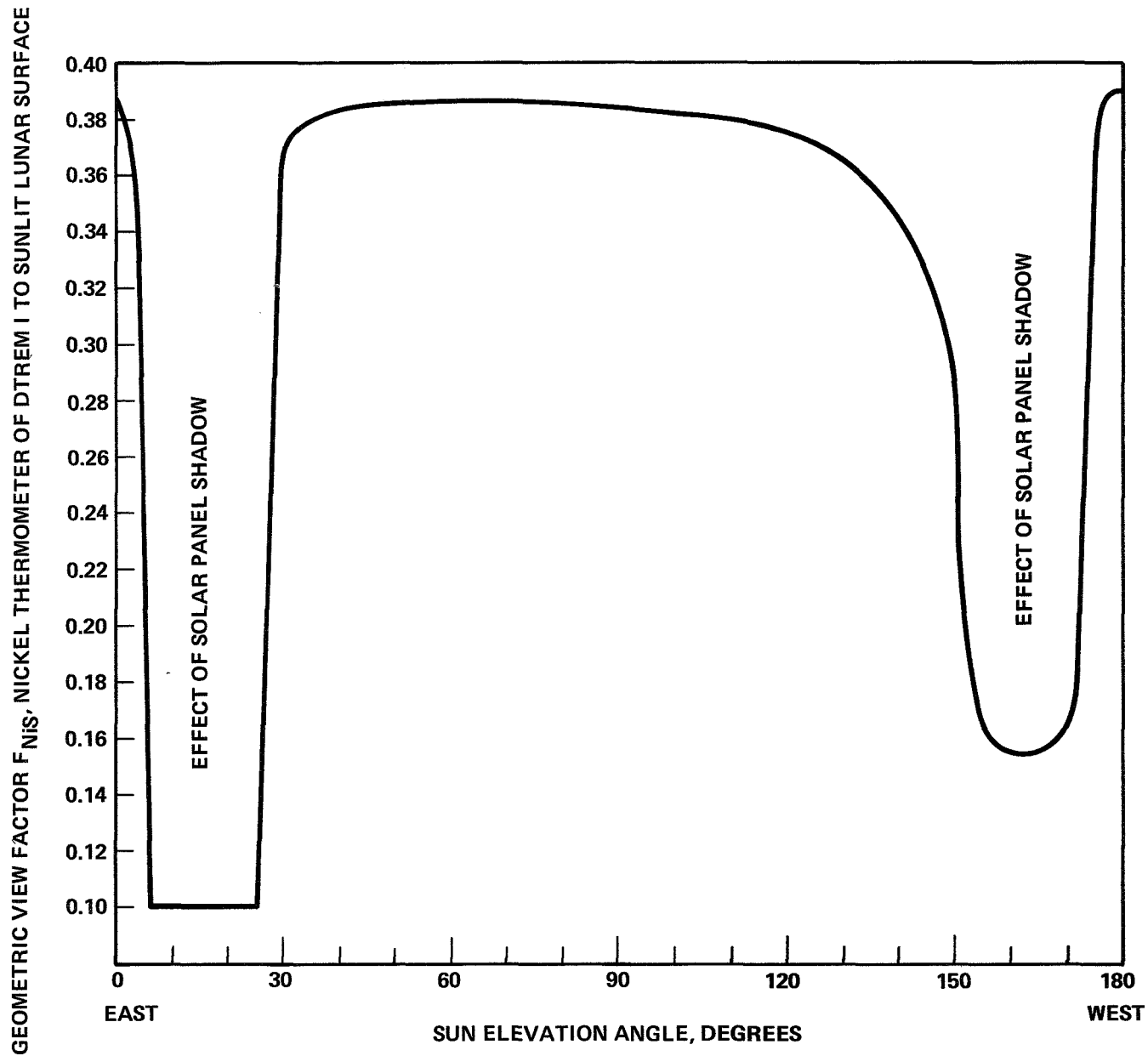


FIGURE 9 - GEOMETRIC VIEW FACTOR F_{NiS} FOR THE THERMAL RADIATION CALCULATION

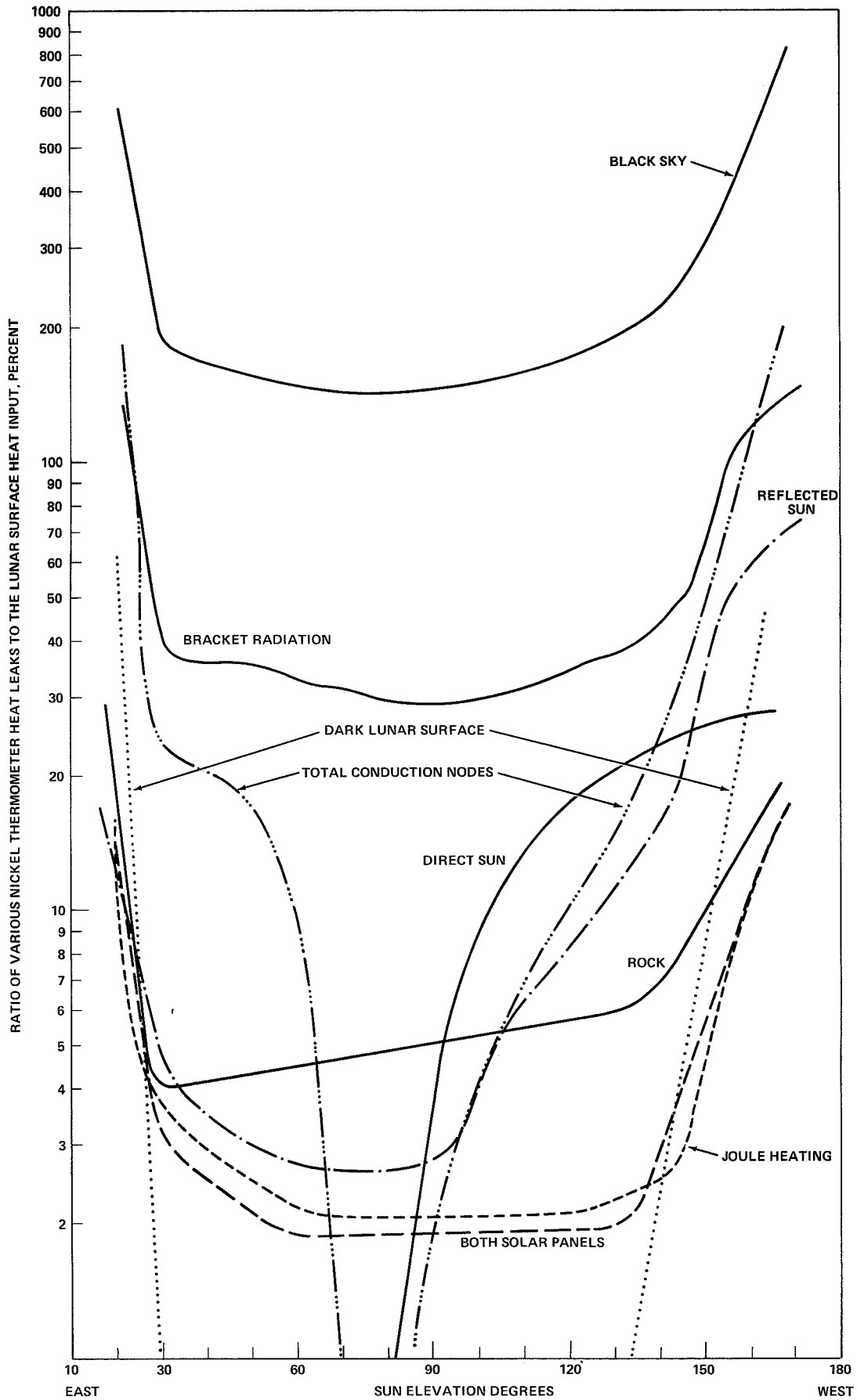


FIGURE 10 - CALCULATED HEAT LEAKS USED IN THE DATA REDUCTION (SEE EQUATION 1).

$$\text{THE LUNAR SURFACE HEAT INPUT IS } \epsilon_{Ni} F_{NiS} \epsilon_S \sigma T_S^4$$

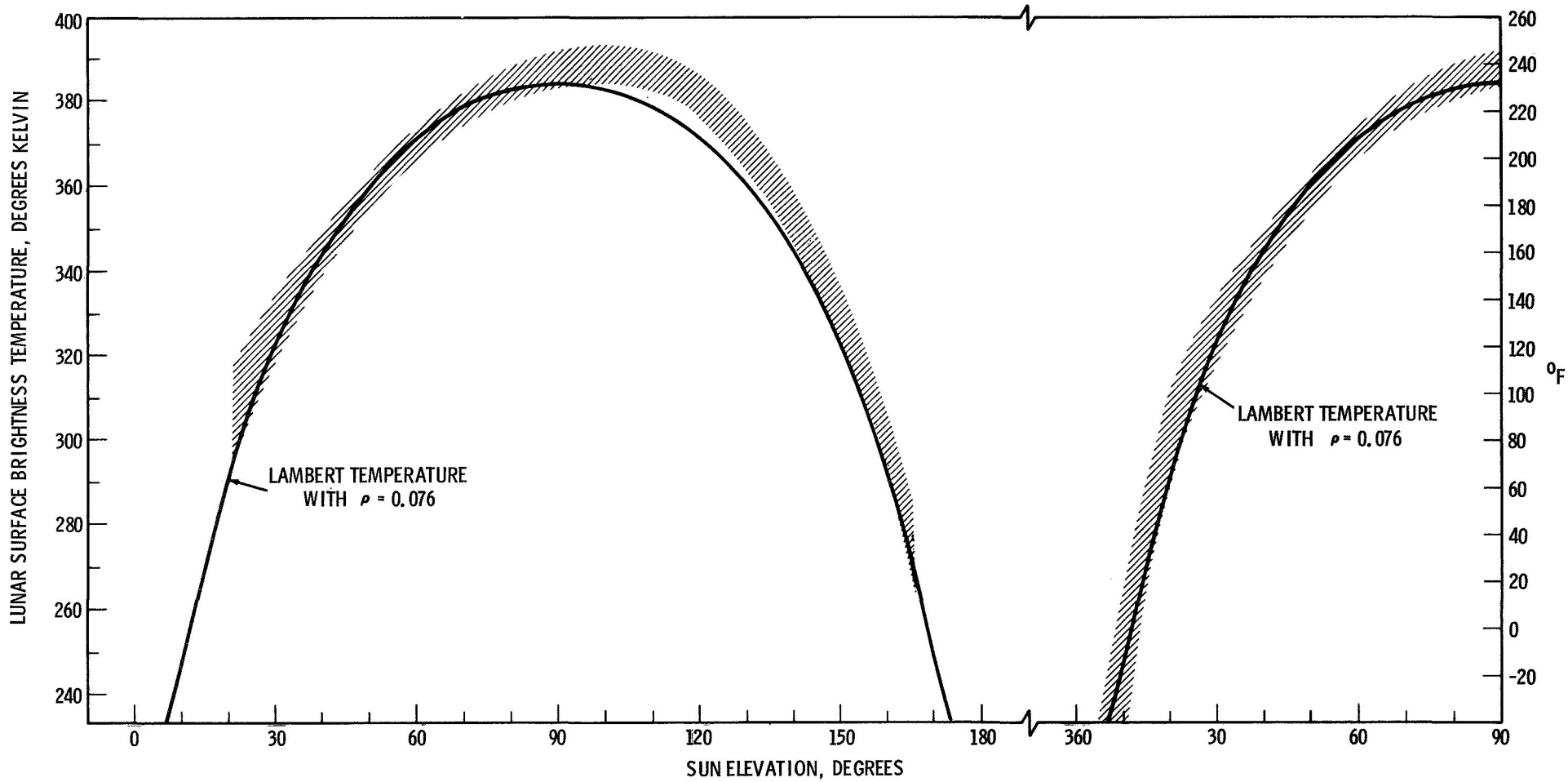


FIGURE 11 - LUNAR SURFACE BRIGHTNESS TEMPERATURE ($\epsilon_s = 1$) INFERRED FROM APOLLO 11 DATA

THE LAMBERT TEMPERATURE IS $[(1 - \rho) S \sin\phi / \sigma]^{1/4}$